Processing and Application of Ceramics 13 [1] (2019) 79–88
https://doi.org/10.2298/PAC1901079L

Investigation of the interactions between titanium and calcium zirconium oxide ($CaZrO_3$) ceramics modified with alumina

Ming-Wei Lu[1], Kun-Lin Lin[2], Chien-Cheng Lin[1,*]

[1]*Department of Materials Science and Engineering, National Chiao-Tung University, Hsinchu, Taiwan*
[2]*National Nano Device Laboratories, National Applied Research Laboratories, Taiwan*

Received 10 August 2018; Received in revised form 13 December 2018; Accepted 13 February 2019

Abstract

Powdered mixtures of CaO, ZrO_2 and Al_2O_3 in various ratios were hot pressed. The mixtures reacted with titanium at 1600 °C for 30 min in argon to evaluate the suitable ceramic crucibles for casting of titanium. The interfacial microstructures between titanium and ceramic composites were characterized using X-ray diffractometer, scanning and transmission electron microscope. The produced hot pressed mixtures that were chemically bonded together, contained calcium aluminate ($CaAl_2O_4$), calcium dialuminate ($CaAl_4O_7$), cubic zirconia (c-ZrO_2), and calcium zirconium oxide ($CaZrO_3$). The increase in Al_2O_3 amount led to the decrease in $CaZrO_3$ amount and an increase in the amount of $CaAl_2O_4$, $CaAl_4O_7$ and c-ZrO_2 due to the reaction of CaO and Al_2O_3. At the end of the reaction of the ceramic mixtures with Ti at 1600 °C for 30 min, the acicular α-Ti and β′-Ti were formed at the interface of Ti and the composites containing up to 10 vol.% Al_2O_3. In composites containing more than 20 vol.% Al_2O_3, Ti_3Al_5 was found at the interface instead of α-Ti and β′-Ti. Furthermore, $CaZrO_3$, ZrO_2 and $Ca_3Al_2O_6$ existed on the sides of the ceramic far away from the interface. $CaZrO_3$/Al_2O_3 composites with less than 20 vol.% Al_2O_3 could be a potential crucible or mould material for productive applications in titanium casting.

Keywords: *titanium casting, CaZrO3, Ca3Al2O6, microstructure, phase identification*

I. Introduction

Titanium and its associated alloys possess high tensile strength, excellent toughness and light weight [1]. There are some advantages of titanium over other metals: titanium has very high corrosion resistance and it is widely used in aerospace, jet engines, medical devices, computer industry and in the manufacturing of consumable parts, such as bicycle parts and the head of a golf club [2,3]. Titanium tends to react with ceramic crucible in the vacuum through induction melting [4]. Hence, titanium alloys are subjected to melting in a water-cooled copper crucible by the consumable electrode vacuum arc melting (VAR) technique [5]. However, there are some disadvantages of the VAR process, such as the high cost of VAR equipment, challenges associated with the recycling of scrap, and long cycle time. Furthermore, an abundant oxygen layer on the surface of titanium, called "α-case" occurs as a result of the reaction between the oxide on the surface of the crucibles and titanium during casting. The α-case will lead to degradation of titanium's surface, hence, causing a deterioration in the mechanical properties of titanium. Therefore, the concept of determining how to control the interfacial reactions between molten titanium and some ceramic materials is of great interest.

Refractory materials, such as Y_2O_3, CaO and ZrO_2, have been investigated as crucible materials for melting titanium alloys. In the past few decades, extensive studies have been conducted with regard to interfacial reactions between molten titanium and zirconia moulds and/or crucibles [6–13]. Saha and Jacob [9] indicated that a brittle α-case was formed on the surface of titanium, thereby adversely affecting the mechanical properties of titanium. Economos and Kingery [6] discovered that molten titanium could penetrate through the grain boundaries of ZrO_2 to form black oxygen-deficient zirconia. Recently, Lin *et al.* [14–20] thoroughly investigated the phase formation mechanisms and the microstructures formed at the interface be-

* Corresponding author: tel: +886 3 5712121 #55370,
e-mail: *chienlin@faculty.nctu.edu.tw*

tween titanium (or titanium alloys) and 3Y-ZrO_2 (or varying Y_2O_3/ZrO_2 ratios) using analytical electron microscopy. Both lamellar orthorhombic Ti_2ZrO and spherical hexagonal Ti_2ZrO were found in α-Ti(Zr,O) after the reaction at 1550 °C [17,19,20]. Lin and Lin [18] also found intergranular α-Zr, twinned t'-ZrO_{2-x}, lenticular t-ZrO_{2-x}, and ordered c-ZrO_{2-x} on the zirconia side far from the interface between Ti and 3Y-ZrO_2, after annealing at 1550 °C. The ZrO_2 was dissolved into Ti on the zirconia side near the original interfaces; Y_2O_3 precipitates in the samples containing 30–70 vol.% Y_2O_3 [21]. Furthermore, the Y_2O_3/ZrO_2 samples became more stable with increasing Y_2O_3 because the solubility of Y_2O_3 in Ti was very low.

As for CaO-ZrO_2 system, Kim *et al.* [22,23] demonstrated that the surface coating of $CaZrO_3$ on to the crucibles is suitable for Ti alloys casting. The $CaZrO_3$ possesses comparable chemical properties to ZrO_2 because $CaZrO_3$ is chemically inert to ZrO_2 and has lower cost compared to yttria-based systems. Thus, $CaZrO_3$ could be a potential refractory material for titanium casting. According to Chang and Lin [24], a diffusion zone featuring columnar $CaZrO_3$ was formed after reaction of Ti and CaO/ZrO_2 composites at 1550 °C. The $CaZrO_3$ was formed due to the outward diffusion of oxides and zirconia away from fully stabilized ZrO_2. This result indicates that $CaZrO_3$ was in a stable phase and it was not significantly dissolved in Ti. Furthermore, Lin *et al.* [25] studied $CaZrO_3$ as a crucible for Ti-6Al-4V (or TC4) and TiNi-alloy based melts material. Small amount of Ca, Zr, Ti and Ni diffused to the original interfacial reaction layer, indicating that $CaZrO_3$ has a promising performance and a very good refractory resistance [25]. In Schafföner *et al.* study [26], $CaZrO_3$ crucible was able to withstand Ti-6Al-4V and TiAl melts, thereby not exhibiting any form of cracking due to the low thermal shock resistance.

The $CaZrO_3$ mixed with Al_2O_3, Y_2O_3, and MgO possess high chemical stability and a very good tolerance against thermal shock [27]. The $CaZrO_3/Al_2O_3$ samples contained Al_2O_3 in various quantities, i.e. 10, 20, 30, and/or 40 vol.% of Al_2O_3 and the equimolar ratio (1 : 1) of CaO and ZrO_2 powders in a balanced reaction with commercially pure titanium (Cp-Ti) melt at 1600 °C in 30 min. The macrostructures were characterized using X-ray diffractometer (XRD), scanning electron microscope (SEM), and transmission electron microscope (TEM) with an attached energy-dispersive X-ray spectroscope (EDS). The phase formation mechanism and microstructural evolution between Cp-Ti and $CaZrO_3/Al_2O_3$ composites were elucidated.

II. Experimental procedure

Ceramic composites were prepared from powdered zirconia (> 99.9 wt.% ZrO_2; the average particle size was smaller than 0.5 μm; Toyo Soda Mfg. Co., Tokyo, Japan), calcia (> 99.9 wt.% CaO 0.5 μm average particle size; Sigma Aidrich, Missouri, United States), and α-alumina (> 99.9 wt.% Al_2O_3; ≤ 10 μm average particle size; Sigma Aidrich, Missouri, United States). Powder mixtures of ZrO_2 and CaO containing 10, 20, 30, and 40 vol.% Al_2O_3 were prepared and designated as CZA10, CZA20, CZA30, CZA40, respectively. Ceramic powder mixtures were dispersed in ethanol and the pH of the suspension was adjusted to 11 by adding 0.2–0.7 wt.% ammonium hydroxide (NH_4OH). The suspension was subjected to ultrasonic vibration for 10 min, dried in an oven at 150 °C, ground with an agate mortar and pestle, and screened through an 80 mesh (sieve size is 0.177 mm). Bulk ceramic composites were fabricated by hot pressing in a graphite furnace at 1 atm argon. Then, the composite specimens were heated at 300 °C and held for 3 min under 5 MPa at a heating rate of 30 °C/min, followed by heating to 1300 °C and holding for 30 min under 30 MPa at a heating rate of 25 °C/min. During cooling, pressure was released at 1100 °C. The phase identification of $CaZrO_3/Al_2O_3$ composites was performed by XRD.

The apparent densities and bulk densities of hot pressed $CaZrO_3/Al_2O_3$ samples were determined by the Archimedes principle using water as an immersion medium. The hot press conditions, compositions, relative densities, and designations of $CaZrO_3/Al_2O_3$ samples are listed in Table 1. The relative densities of the CZ (pure $CaZrO_3$), CZA10, CZA20, CZA30 and CZA40 were 98.0, 98.5, 98.2, 98.3 and 98.6% TD, respectively.

Hot pressed ceramic composites were cut and machined to the dimensions of about 10 mm × 10 mm × 5 mm. The composite $CaZrO_3/Al_2O_3$ was placed into the graphite crucible and tightly packed with commercially pure titanium powder. The crucible was placed in an electric resistance furnace having its heating elements made of tungsten. The chamber was evacuated at vacuum of about 10^{-4} torr and refilled with argon. The cycle of vacuum evacuation and purging with argon was repeated three times. The temperature was increased to 1600 °C at a heating rate of 10 °C/min, where the composites were held at 1600 °C for 30 min and cooled to room temperature in the furnace.

The phase identification was performed using an XRD Model D8 DISCOVER, Bruker AXS, Germany). The operating conditions of X-ray diffraction were CuKα radiation at 40 kV and 40 mA, and a scanning rate of 1.2°/min. SEM (Model JSM 6500F, JEOL Ltd., Japan) was used for the microstructural observation of the interfaces between Ti and $CaZrO_3/Al_2O_3$ samples. SEM specimens were cut and ground using a diamond matted disc, and polished using diamond pastes of sizes 6, 3, and 1 μm in sequence. The TEM specimens were prepared by focused ion beam (FIB) so that the thickness is less than 100 nm. Prior to the FIB milling, a layer of platinum approximately 1 μm thick was deposited on the specimen by ion beam chemical deposition using Trimethyl-methylcyclopentadienyl-platinum(IV) ($C_9H_{16}Pt$) as a precursor gas. The Pt layer served as

a marker and prevented the outer surface of the sample from being directly exposed to the gallium ion beam implantation during subsequent ion milling operations. The FIB milling was performed with a Ga^+ ion beam at 30 keV. After rough milling (7–1 nA), polishing (0.5–0.1 nA), and final polishing (50–10 pA), a thin foil of (17 μm × 2 μm × 0.05 μm) was cut off and transferred to a TEM grid (Formvar/Carbon Coated-Copper 200 mesh) using a micromanipulator for subsequent TEM analyses.

The interfacial microstructures were then characterized using a TEM (Model JEM 2010F, JEOL Ltd.) equipped with an EDS (OXFORD INCA, X-Max^N Silicon Drift Detector, Oxford Instrument Inc.). The analyses of atomic configurations in various phases were performed using a computer simulation software for crystallography (CaRIne Crystallography 3.1, Divergent S.A., Compiegne, France). Chemical quantitative analyses for various phases were conducted by the Cliff-Lorimer standardless technique [28]. A conventional ZAF correction was done using the LINK ISIS software.

III. Results and discussion

3.1. $CaZrO_3/Al_2O_3$ composites

Figure 1 shows the XRD spectra of various hot pressed $CaZrO_3/Al_2O_3$ samples. Two phases, orthorhombic $CaZrO_3$ (calcium zirconate) and cubic zirconia (c-ZrO_2), were found in CZ sample. When Al_2O_3 was added to the composites, calcium aluminate ($CaAl_2O_4$) or calcium dialuminate ($CaAl_4O_7$) were formed, in addition to c-ZrO_2 and $CaZrO_3$. The amount of c-ZrO_2 increases with increasing amount of Al_2O_3 in the composites as indicated by the peak at 30° of XRD spectra. Furthermore, the amount of $CaZrO_3$ decreases with increasing amount of Al_2O_3. The XRD results were consistent with the phases indicated by the CaO-Al_2O_3-ZrO_2 phase diagram at 1380 °C [29] and are listed in Table 1.

Figure 2 shows the backscattered electron images (BEI) of various $CaZrO_3/Al_2O_3$ samples after they have been hot pressed at 1300 °C for 30 min. The EDS analyses showed that the bright area was identified as c-ZrO_2, the grey area was identified as $CaZrO_3$, and the dark portion of the grains was identified as $CaAl_2O_4$. Obvi-

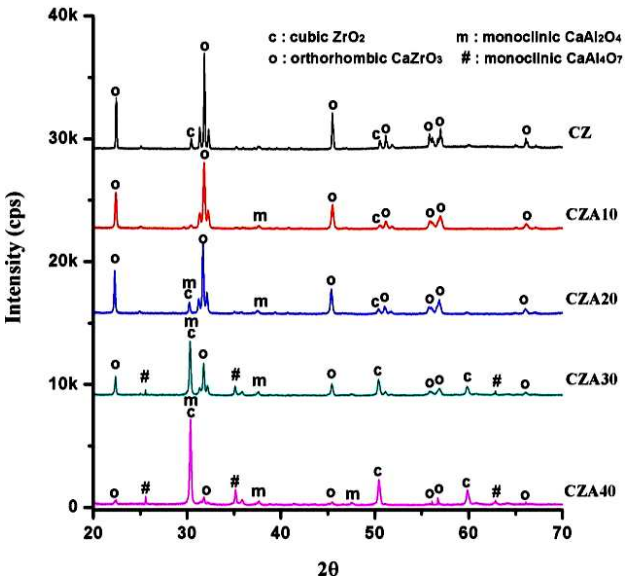

Figure 1. X-ray diffraction spectra of hot pressed $CaZrO_3/Al_2O_3$ composites

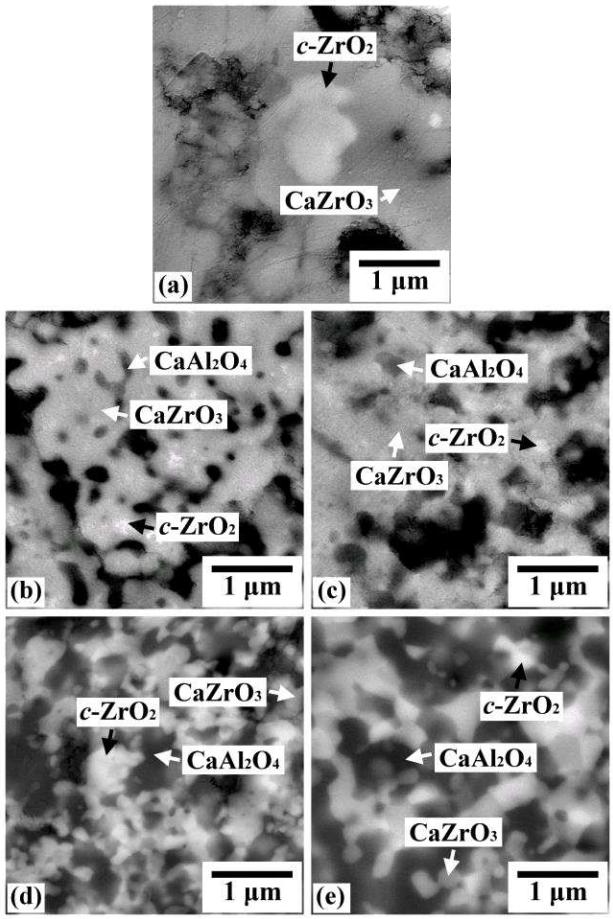

Figure 2. BEI of scanning electron microscopy of: a) CZ, b) CZA10, c) CZA20, d) CZA30, and e) CZA40 after hot pressing the composite at 1300 °Cfor 30 min

Table 1. Designations, compositions, relative density (δ) and XRD phases of hot pressed $CaZrO_3/Al_2O_3$ samples

Specimens	Composition [vol.%]	δ [%TD]	XRD phases
CZ	44.45% CaO + 55.55% ZrO_2	98.0	$CaZrO_3$, c-ZrO_2
CZA10	10% Al_2O_3 + 90% (CaO/ZrO_2)	98.5	$CaZrO_3$, c-ZrO_2, $CaAl_2O_4$
CZA20	20% Al_2O_3 + 80% (CaO/ZrO_2)	98.2	$CaZrO_3$, c-ZrO_2, $CaAl_2O_4$
CZA30	30% Al_2O_3 + 70% (CaO/ZrO_2)	98.3	$CaZrO_3$, c-ZrO_2, $CaAl_2O_4$, $CaAl_4O_7$
CZA40	40% Al_2O_3 + 60% (CaO/ZrO_2)	98.6	$CaZrO_3$, c-ZrO_2, $CaAl_2O_4$, $CaAl_4O_7$

ously, there were pores in CZ and CZA10 (Figs. 2a,b). When the content of Al_2O_3 in the composites was increased, the pores disappeared in CZA30 and CZA40 (Figs. 2d,e). Thus, the addition of Al_2O_3 improves densification of the composites due to the formation of calcium aluminate or calcium dialuminate and elimination of the pores.

The addition of divalent oxide (CaO and MaO) and trivalent oxide (Sc_2O_3, Y_2O_3, Al_2O_3) into zirconia can result in c-ZrO_2 due to the formation of oxygen vacancies [17,21,24]. As for calcium zirconate ($CaZrO_3$), the CaO reacts with ZrO_2 to form $CaZrO_3$ as demonstrated by the negative free energy in Eq. 1 [30]:

$$CaO + ZrO_2 \rightarrow CaZrO_3 \ \Delta G = -54 \sim -71\ \text{kJ/mol} \quad (1)$$

The free energies of the calcium aluminate phases, including $CaAl_2O_4$, $CaAl_4O_7$ and $Ca_{12}Al_{14}O_{33}$, are shown in Eqs. 2–7 [31,32]:

$$Al_2O_3 + CaO \rightarrow CaAl_2O_4 \ \Delta G = -38\ \text{kJ/mol} \quad (2)$$

$$2\,Al_2O_3 + CaO \rightarrow CaAl_4O_7 \ \Delta G = -51\ \text{kJ/mol} \quad (3)$$

$$7\,Al_2O_3 + 12\,CaO \rightarrow Ca_{12}Al_{14}O_{33} \ \Delta G = -275\ \text{kJ/mol} \quad (4)$$

$$Ca_{12}Al_{14}O_{33} + 17\,Al_2O_3 \rightarrow 12\,CaAl_4O_7 \ \Delta G = -26\ \text{kJ/mol} \quad (5)$$

$$Ca_{12}Al_{14}O_{33} + 5\,Al_2O_3 \rightarrow 12\,CaAl_2O_4 \ \Delta G = -14\ \text{kJ/mol} \quad (6)$$

$$Ca_{12}Al_{14}O_{33} + {}_5CaAl_4O_7 \rightarrow 12\,CaAl_2O_4 \ \Delta G = -7\ \text{kJ/mol} \quad (7)$$

From the calculation of the Gibbs free energies of calcium aluminate phases, the most negative free energy was that of $Ca_{12}Al_{14}O_{33}$, showing that the reaction is the most spontaneous when compared to the free energies of $CaAl_2O_4$ and $CaAl_4O_7$. However, $Ca_{12}Al_{14}O_{33}$ phase was not part of the present study. Possibly, the $Ca_{12}Al_{14}O_{33}$ phase reacted with Al_2O_3 to form $CaAl_4O_7$ and $CaAl_2O_4$ as shown in Eqs. 5 and 6, or the $Ca_{12}Al_{14}O_{33}$ phase might have reacted with $CaAl_4O_7$ to form $CaAl_2O_4$ as indicated by Eq. 7. It is also possible that the $Ca_{12}Al_{14}O_{33}$ phase was a transient phase, which was not observed in the study. In addition, $CaAl_2O_4$ was the main phase instead of $CaAl_4O_7$, although the free energy of $CaAl_4O_7$ was smaller than that of the $CaAl_2O_4$ phase. $CaAl_4O_7$ could react with $Ca_{12}Al_{14}O_{33}$ phase to form $CaAl_2O_4$ phase as indicated by the Eq. 7 and reported by Iftekhar *et. al.* [32].

3.2. Reactions of Cp-Ti with $CaZrO_3/Al_2O_3$

Figures 3a-e display the cross sectional BEI of Ti and various composites of $CaZrO_3/Al_2O_3$ after the occurrence of a reaction at 1600 °C for 30 min. Titanium is shown at the left of each micrograph, while the ceramic sample is on the right-hand side. Reaction layer I on the metal side close to the original interface is marked as "I" in Figs. 3a-e, while reaction layer II on the ceramic side close to the original interface is marked as "II". The zone within the ceramic side that is affected by the interfacial reaction is marked as 'III". Arrows indicating the original interface are shown on the diagram according to the characteristic Kα X-ray maps of calcium (not shown), since Ca is relatively insoluble in Ti with respect to zirconium, oxygen and aluminium. The large pores in the interface near the ceramics, as shown in the region II, could be attributed to the Kirkendall effect be-

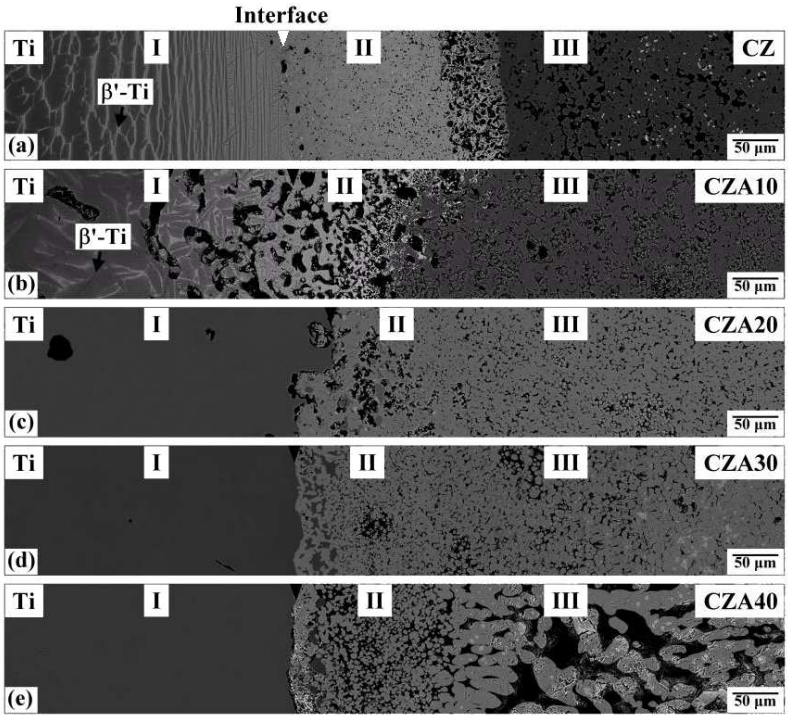

Figure 3. BEI images of: a) CZ, b) CZA10, c) CZA20, d) CZA30, and e) CZA40, showing the cross section between Ti and $CaZrO_3/Al_2O_3$ composites after the reaction at 1600 °C for 30 min (arrows indicate the original interface between Ti and $CaZrO_3/Al_2O_3$ composites)

cause zirconium and oxygen must have diffused to the titanium side more rapidly than the rate of diffusion of titanium into the ceramic side.

Reaction layer "I" - at the titanium side

Reaction layer "I" contains dark needle-like regions and bright regions near the interfaces of Ti/CZ and Ti/CZA10, as shown in Figs. 3a,b. The needle-like regions should be α-Ti(Zr,O) phase and the bright regions should be the β'-Ti(Zr,O) phase, which conforms to the previous reports by Lin and Lin studies [17,19,20]. The needle-like α-Ti(O) phase and the β'-Ti(Zr,O) phase are usually found in the titanium side of the micrograph because of the interfacial reactions between Ti and 3Y-ZrO_2. An α-Ti(O) phase with a small amount of oxygen in solid solution and β'-Ti(Zr,O) dissolved a significant amount of zirconium (β stabilizer) and oxygen (α stabilizer) in solid solution [17,19,20]. Moreover, the needle-like α-Ti(O) and β'-Ti(Zr,O) in reaction layer "I" were effectively suppressed at the titanium side of Ti/CZA20, Ti/CZA30 and Ti/CZA40.

Reaction Layer "II" - near the interface

BEI images of reaction layer "II" in the ceramic side of Ti/CZ, Ti/CZA10, Ti/CZA20, Ti/CZA30 and Ti/CZA40 after reaction at 1600 °C for 30 min are shown in Fig. 4. After reaction at 1600 °C for 30 min, a large amount of titanium diffused to the region occupied by ZrO_2 and $CaZrO_3$. The diffused titanium was also involved in a reaction with both ZrO_2 and $CaZrO_3$ of Ti/CZ and Ti/CZA10 composites to form acicular α-Ti(Zr,O), β'-Ti(Zr,O) and residual $CaZrO_3$, as shown in Figs. 4a,b. Furthermore, the precipitation of the needle-like α-Ti(Zr,O) solid solution on the β'-Ti(Zr,O) substrate during the cooling process was very common at the interfacial reactions between Ti and ZrO_2 [17,19,21,24]. However, two phases of α-Ti(Zr,O) and β'-Ti(Zr,O) in reaction layer "II" were found when Al_2O_3 content increased above 20 vol.%. Titanium was involved in the reaction with Al from liquid $CaAl_2O_4$ (melting point ~1604 °C, which is close to the reacting temperature of 1600 °C) to form Ti_3Al_5. The formation mechanism for Ti_3Al_5 is shown in the equation below:

$$3\,Ti + 5\,Al \rightarrow Ti_3Al_5 \quad (8)$$

Meanwhile, the ZrO_2 at reaction layer "II" was dissolved in Ti_3Al_5, which is supported by the EDS analysis (32.77 at.% Ti, 52.85 at.% Al, 8.40 at.% Zr, 4.71 at.% O, 1.27 at.% Ca). Besides, when Al_2O_3 content increased above 30 vol.% in Figs. 4d,e, the morphology of both Ti_3Al_5 and $CaZrO_3$ changed into smooth and spherical shapes due to the formation of a large amount of liquid $CaAl_2O_4$. In addition to the Ti_3Al_5 phase, the $Ca_3Al_2O_6$ phase was also found as shown in Figs. 4b-e. The formation mechanism of $Ca_3Al_2O_6$ phase could be described as follows:

$$CaAl_2O_4 + 2\,CaZrO_3 \rightarrow Ca_3Al_2O_6 + 2\,ZrO_2 \quad (9)$$

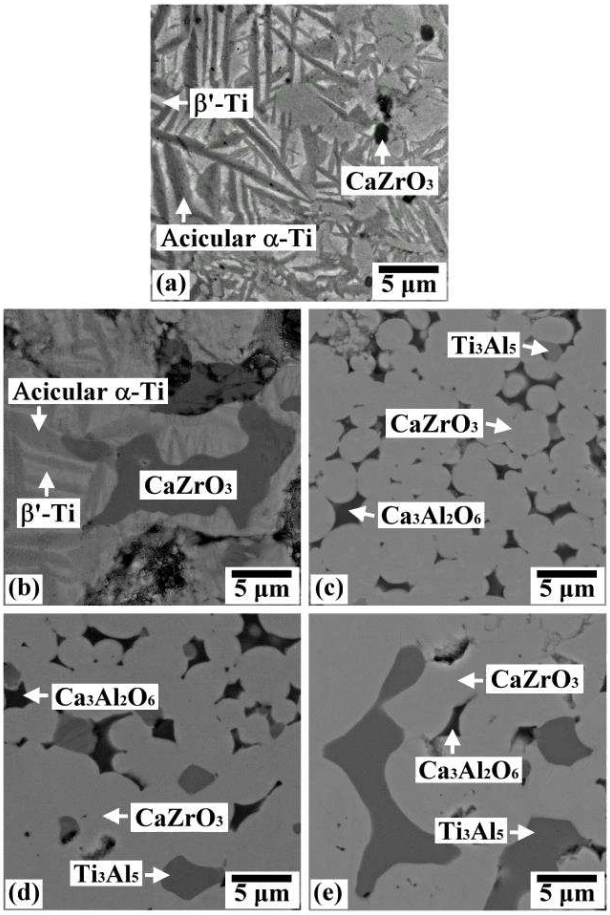

Figure 4. BEI of scanning electron microscopy in the reaction layer "II" of the ceramic side at the interface between Ti and: a) CZ, b) CZA10, c) CZA20, d) CZA30, and e) CZA40 after the reaction at 1600 °Cfor 30 min

The phase identification for $Ca_3Al_2O_6$ is discussed in the TEM analysis below.

Figure 5 shows the bright field images (BFI), selected area diffraction patterns (SADPs), and EDS of $CaZrO_3$ and Ti_3Al_5 in reaction layer "II" of Ti/CZA40 after the reaction at 1600 °C for 30 min. Figures 5b,c show the SADPs of $CaZrO_3$ with $[\bar{1}01]$ and $[\bar{2}01]$ zone axes, respectively. The lattice parameters of the $CaZrO_3$ phase were measured and calculated to be a = 5.59 Å, b = 8.17 Å, c = 5.95 Å, and $\alpha = \beta = \gamma = 90°$, which corresponded to the parameters of the orthorhombic $CaZrO_3$ reported in JCPDS# 350790 (a = 5.7558 Å, b = 8.0101 Å, c = 5.5929 Å, $\alpha = \beta = \gamma = 90°$, space group is *Pmna*). The EDS spectrum in Fig. 5d showed that $CaZrO_3$ dissolved a small amount of Ti and Al (27.05 at.% Zr, 20.68 at.% Ca, 51.6 at.% O, 0.31 at.% Al and 0.36 at.% Ti). Figures 5e,f show the SADPs of Ti_3Al_5 with $[0\bar{1}0]$ and $[0\bar{1}2]$ zone axes, respectively. The lattice parameters of the Ti_3Al_5 phase were measured and calculated to be $a = b$ = 11.52 Å, c = 4.15 Å, $\alpha = \beta = \gamma = 90°$, which corresponded to the parameters of tetragonal Ti_3Al_5 reported in JCPDS# 420810 ($a = b$ = 11.26 Å, c = 4.02 Å, $\alpha = \beta = \gamma = 90°$, space group is *P4/mbn*). The EDS spectrum in Fig. 5g shows

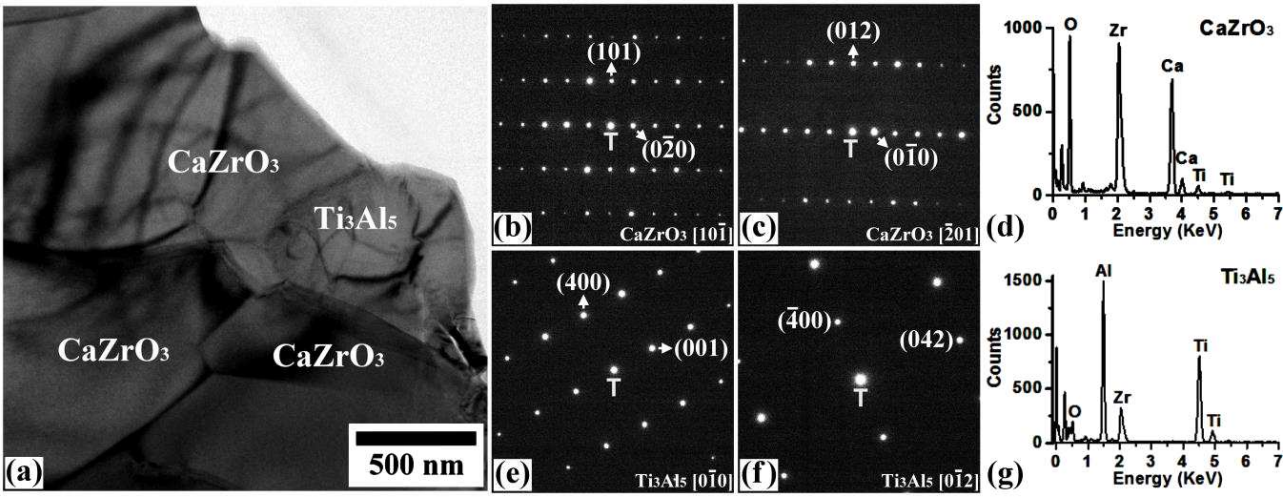

Figure 5. The bright field image of transmission electron microscopy of the reaction layers II at the Ti/CZA40 after reaction at 1600 °C for 30 min (a); SADPs of $CaZrO_3$ along the [$\bar{1}$01] (b) and [$\bar{2}$01] zone axes (c); an energy-dispersive spectrum of $CaZrO_3$ (d); an SADP of Ti_3Al_5 along the [0$\bar{1}$0] (e) and [0$\bar{1}$2] zone axes (f); an energy-dispersive spectrum of Ti_3Al_5 (g)

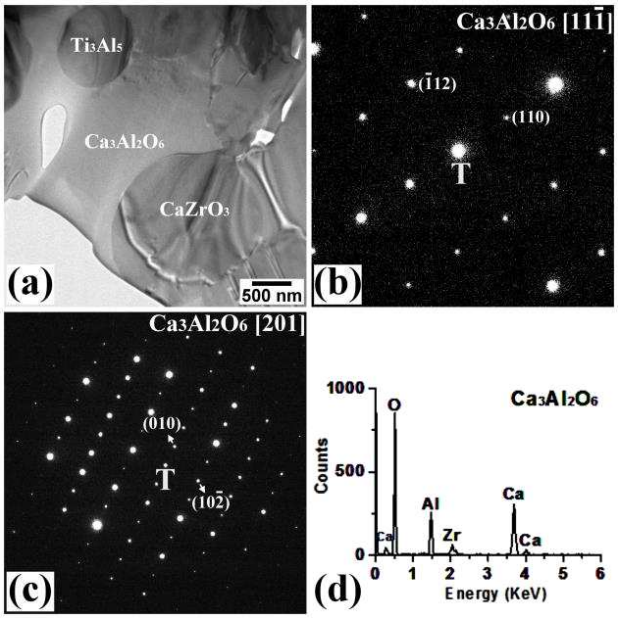

Figure 6. The bright field image of a transmission electron microscopy of reaction layers II and III at the Ti/CZA40 interface after reaction at 1600 °C for 30 min (a); SADPs of $Ca_3Al_2O_6$ along the [11$\bar{1}$] (b) and [201] zone axes (c); an energy-dispersive spectrum of $Ca_3Al_2O_6$ (d)

that the composition of the Ti_3Al_5 was 27.97 at.% Ti, 50.63 at.% Al, 10.91 at.% O and 10.22 at.% Zr.

Figure 6a shows the bright field image between reaction layer "II" and "III" of Ti/CZA40 after reaction at 1600 °C for 30 min. It indicates the formation of Ti_3Al_5, $Ca_3Al_2O_6$ and $CaZrO_3$. Figures 6b,c show the SADPs of $Ca_3Al_2O_6$ with [11$\bar{1}$] and [201] zone axes, respectively. The lattice parameters of the $Ca_3Al_2O_6$ phase were measured and calculated to be a = 10.68 Å, b = 10.85 Å, c = 15.34 Å, and $\alpha = \beta = \gamma = 90°$, which correspond to the parameters of the orthorhombic $Ca_3Al_2O_6$ reported in JCPDS# 330251 (a = 10.8737 Å, b = 10.8512 Å, c = 15.1152 Å, $\alpha = \beta = \gamma = 90°$). The EDS spectrum in Fig. 6d shows that $Ca_3Al_2O_6$ is composed of 22.41 at.% Ca, 23.16 at.% Al, 49.67 at.% O and 4.76 at.% Zr.

Reaction Layer "III" - at the composites side

Figures 7a-e display the backscattering electron image of the reaction layer "III" in the Ti/composites joint after reaction at 1600 °C for 30 min. It was observed that the shape of $CaZrO_3$ was changed to spherical form when amount of Al_2O_3 increased above 20 vol.% due to the formation of the liquid phase, i.e. $Ca_3Al_2O_6$. The liquid phase, $Ca_3Al_2O_6$, would penetrate between $CaZrO_3$ grains, exerting an attractive force, thereby pulling the grains together. Furthermore, the content of $Ca_3Al_2O_6$ increases with an increase in the amount of Al_2O_3 on the ceramic side. A large amount of liquid $Ca_3Al_2O_6$ tended to enhance the shrinkage and increase in density of $CaZrO_3$, resulting in the reduction of the pores and grain growth in reaction layer "III". During the reaction, liquid $CaAlO_2$ dissolved $CaZrO_3$ and ZrO_2 at 1600 °C. When the solution reached the saturation concentration, $CaZrO_3$ and ZrO_2 precipitated again in the solution during cooling.

To evaluate the effect of titanium on the composites, the composites were annealed at 1600 °C for 30 min without reacting with titanium. Figure 8 shows the BEI images of the investigated composites after annealing at 1600 °C for 30 min. By the EDS analyses of SEM (not shown), the bright area was identified as c-ZrO_2, the grey area was $CaZrO_3$, and the dark portion of the grains was $CaAl_4O_7$. Obviously, there were lots of pores in the CZ and CZA10 samples (Figs. 8a,b) (arrows in figure). When the content of Al_2O_3 in the composites increased, the pores gradually disappeared and were filled with $CaAl_4O_7$, supported by CZA20, CZA30, and CZA40 specimens (Figs. 8c,d). Thus, the addition of Al_2O_3 contributed to the increase in the density of the composites due to the formation of $CaAl_4O_7$ at 1600 °C.

Figures 9 shows the BFI, SADPs, and EDS of CZA40 after annealing at 1600 °C for 30 min. Figure 9a shows

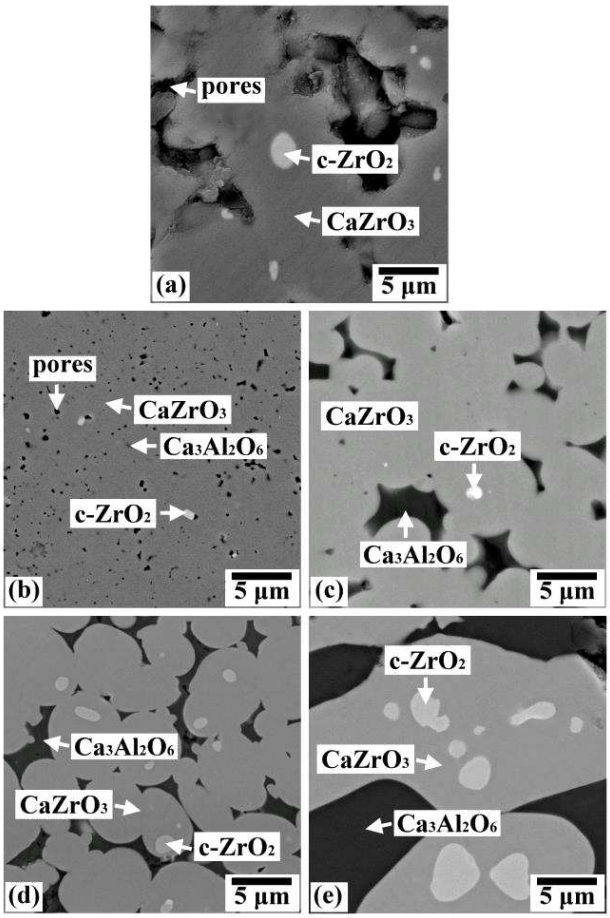

Figure 7. BEI of a scanning electron microscopy of the reaction layer "III" in the ceramic side at the interface between Ti and (a) CZ, (b) CZA10, (c) CZA20, (d) CZA30, and (e) CZA40 after reaction at 1600 °C for 30 min

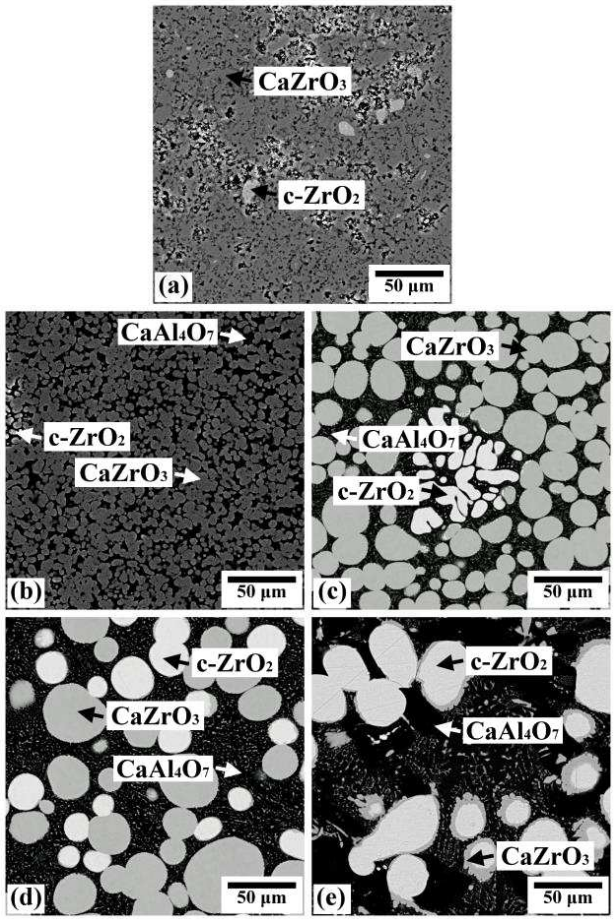

Figure 8. BEI of a scanning electron microscopy of the hot pressed: a) CZ, b) CZA10, c) CZA20, d) CZA30 and e) CZA40 after the heat treatment at 1600 °C for 30 min

presence of c-ZrO_2, $CaAl_4O_7$ and $CaZrO_3$. Figures 9b,c show the SADPs of $CaAl_4O_7$ with [11$\bar{3}$] and [11$\bar{1}$] zone axes, respectively. The lattice parameters of the $CaAl_4O_7$ phase were measured and calculated to be a = 13.27 Å, b = 9.01 Å, c = 6.65 Å, and $\alpha = \gamma = 90° \neq \beta$, which corresponded to the parameters of monoclinic $CaAl_4O_7$ reported in JCPDS# 070082 (a = 12.897 Å, b = 8.879 Å, c = 5.454 Å, $\alpha = \gamma = 90° \neq \beta$, space group is *C2/c*). The EDS spectrum in Fig. 9d shows that $CaAl_4O_7$ composed of 7.12 at.% Ca, 35.01 at.% Al, 57.6 at.% O and 0.18 at.% Zr.

Figure 10 shows the XRD spectra of CZA40 after annealing at 1300 °C, CZA40 after reacting with Ti at 1600 °C, and CZA40 after annealing at 1600 °C in a sequence from the bottom to the top. Four phases, CaZrO (o), c-ZrO_2 (c), $CaAl_2O_4$ (m), and $CaAl_4O_7$ (#) were found both in the CZA40 at 1300 °C and 1600 °C. The amount of $CaAl_4O_7$ increased as indicated by the peak at 21° of XRD spectra and the $CaAl_2O_4$ decreased as indicated by the peak at 37° XRD peak for CZA40 annealed at 1600 °C. The formation mechanism for the $CaAl_4O_7$ could be described as the Eq. 10:

$$2\,CaAl_2O_4 + ZrO_2 \rightarrow CaAl_4O_7 + CaZrO_3 \qquad (10)$$

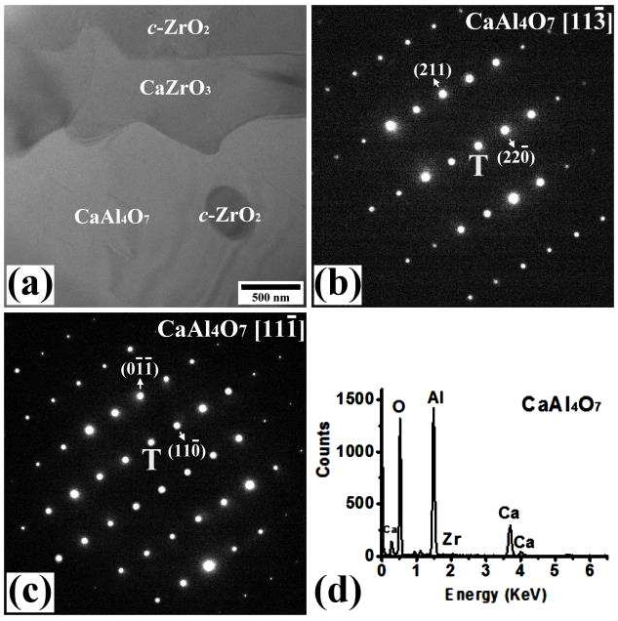

Figure 9. The bright field image of a transmission electron microscopy of the CZA40 after annealed at 1600 °C for 30 min (a); SADPs of $CaAl_4O_7$ along the [11$\bar{3}$] (b) and [11$\bar{1}$] zone axes (c); an energy-dispersive spectrum of $CaAl_4O_7$ (d)

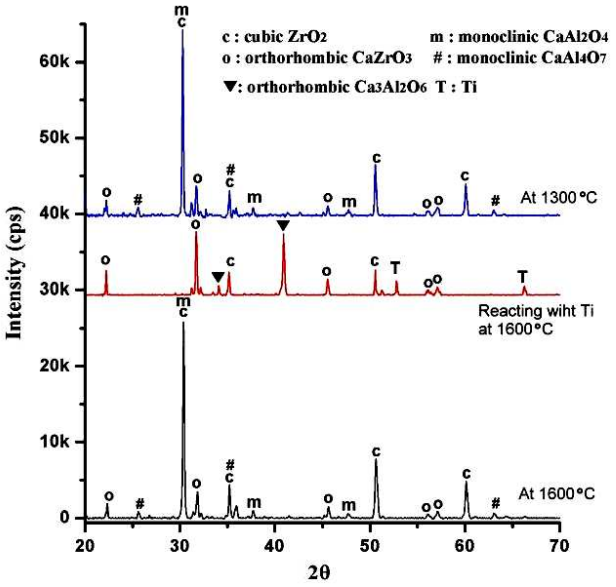

Figure 10. XRD spectra of the CZA40 after hot pressing at 1300 °C, CZA40 after reacting with Ti at 1600 °C, and the hot pressed CZA40 after annealing at 1600 °C

However, when CZA40 undergoes a reaction with Ti, both $CaAl_4O_7$ and $CaAl_2O_4$ disappear leaving behind the $Ca_3Al_2O_6$ phase (▼).

Figure 11a displays the proposed model of microstructural evolution in reaction layers II and III in Ti/CZ at 1600 °C for 30 min. Before hot pressing, the composite is composed of ZrO_2, $CaZrO_3$ and minor pores, but after hot pressing near the interface of reaction layer "II", titanium diffuses into the composite and dissolves a relatively large amount of O and Zr to form β-Ti(Zr,O) solid solution. As the solubility of Ca in Ti was quite limited, Ca was retained in the original $CaZrO_3$. After cooling, the precipitation of the needle-like α-Ti(Zr,O) solid solution occurred on the β'-Ti(Zr,O) substrate. As for reaction layer "III", which is the ceramic side located slightly away from the interface, the phases were ZrO_2, $CaZrO_3$, and minor pores formed after cooling. Figure 11b shows the formation mechanism for reaction layers II and III in the Ti/CZ-Al_2O_3 additive at 1600 °C for 30 min. Before hot pressing, the composite is made of ZrO_2, $CaZrO_3$, $CaAl_2O_4$, $CaAl_4O_7$ and minor pores after hot pressing. When the volume percentage of Al_2O_3 increased above 20 vol.%, Ti tends to diffuse toward the composites and a reaction occurs between titanium and aluminium present in the liquid $CaAl_2O_4$ to form Ti_3Al_5 close to the reaction layer "II". After cooling, the formation of $Ca_3Al_2O_6$ occurs due to $CaZrO_3$ reacting with liquid $CaAl_2O_4$. At some distance slightly away from the ceramic side (reaction layers "III") ZrO_2, $CaZrO_3$ and $Ca_3Al_2O_6$ were found and no Ti_3Al_5 was formed. The reaction layers of each of the samples and their corresponding crystal phases are all marked in Table 2.

IV. Conclusions

1. Ceramic composites of CaO, ZrO_2 and Al_2O_3 in various ratios were used with titanium at 1600 °C for 30 min in Ar. The interfacial microstructures between titanium and ceramic composites were characterized by using XRD, SEM and TEM.
2. Before the addition of titanium, calcium aluminate ($CaAl_2O_4$) or calcium dialuminate ($CaAl_4O_7$), c-

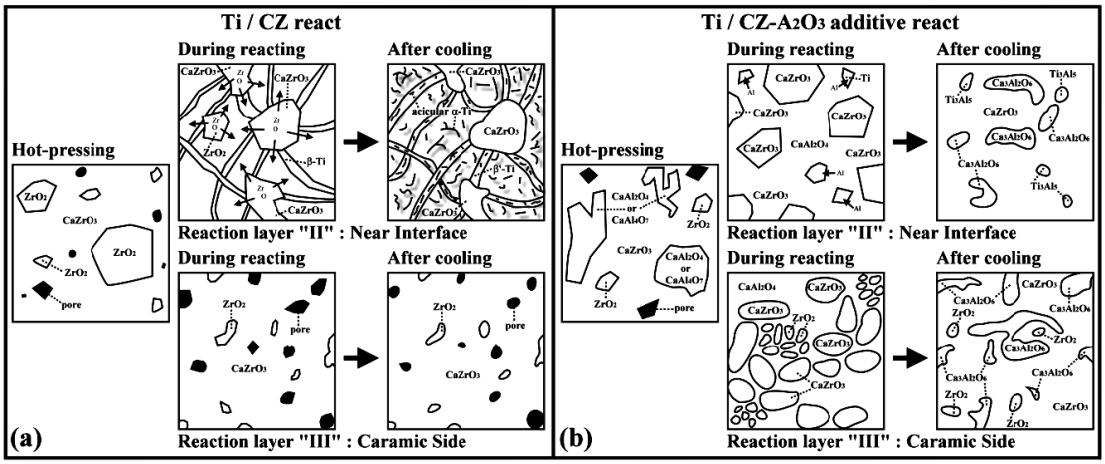

Figure 11. Schematic showing the microstructural evolution of reaction layer "II" and "III' in: a) Ti/CZ and b) Ti/CZ-Al_2O_3 additive

Table 2. Reaction phases at the interface of Ti and $CaZrO_3/Al_2O_3$ composites after the reaction at 1600 °C for 30 min

Specimens	Reaction layers I	Reaction layers II	Reaction-affected zone (III)
Ti/CZ	α-Ti, β-Ti	acicular α-Ti, β'-Ti, $CaZrO_3$	$CaZrO_3$
Ti/CZA10	α-Ti, β-Ti	acicular α-Ti, β'-Ti, $CaZrO_3$	$CaZrO_3$
Ti/CZA20	α-Ti	$CaZrO_3$, $Ca_3Al_2O_6$, Ti_3Al_5	$CaZrO_3$, $Ca_3Al_2O_6$
Ti/CZA30	α-Ti	$CaZrO_3$, $Ca_3Al_2O_6$, Ti_3Al_5	$CaZrO_3$, $Ca_3Al_2O_6$, c-ZrO_2
Ti/CZA40	α-Ti	$CaZrO_3$, $Ca_3Al_2O_6$, Ti_3Al_5	$CaZrO_3$, $Ca_3Al_2O_6$, c-ZrO_2

ZrO_2 and $CaZrO_3$ were formed in the ceramic composites. The amount of $CaZrO_3$ was reduced with an increase in the amount of Al_2O_3 in the composites. Meanwhile, the amounts of calcium aluminate ($CaAl_2O_4$), calcium dialuminate ($CaAl_4O_7$) and c-ZrO_2 increase with an increase in the amount of Al_2O_3 due to the abundance of CaO to react with Al_2O_3.

3. After joining titanium and ceramic composites, the acicular α-Ti and β'-Ti are formed at the interface of the ceramic composites with 0 and 10 vol.% Al_2O_3. When the amount of Al_2O_3 in the ceramic composites exceeded 20 vol.%, the Ti_3Al_5 was formed at the interface rather than α-Ti and β'-Ti. Far from the interface, three phases of $CaZrO_3$, ZrO_2 and $Ca_3Al_2O_6$ existed in the ceramic side. In addition, the pores gradually disappeared on the ceramic side due to the formation of $Ca_3Al_2O_6$.
4. The incorporation of more than 20 vol.% Al_2O_3 in $CaZrO_3/Al_2O_3$ ceramic composites significantly suppressed the formation of the reactional phases at the interface at 1600 °C for 30 min. Conversely, an extensive reaction occurred at the interface between Ti and CZ as well as CZA10. Thus, $CaZrO_3/Al_2O_3$ ceramic composites with more than 20 vol.% Al_2O_3 could be suitable for the titanium casting.

Acknowledgement: The authors gratefully acknowledge the skilful contribution of Mr. C. Capiani (CNR-ISTEC) for the preparation of the samples. This work was partially supported by the ANTENNA project, contract n. 1466.

References

1. R.R. Boyer, "Attributes, characteristics, and applications of titanium and its alloys", *JOM*, **62** [5] (2010) 21–24.
2. C.S. Shira, F.H. Froes, "Advanced materials in golf clubs: The titanium phenomenon", *JOM*, **49** [5] (1997) 35–37.
3. C. Shira, F.H.S. Froes, "Titanium golf clubs", *MRS Bulletin*, **23** [3] (2013) 42–46
4. K. Sakamoto, K. Yoshikawa, T. Kusamichi, T. Onoye, "Changes in oxygen contents of titanium aluminides by vacuum induction, cold crucible induction and electron beam melting", *Trans. Iron Steel Ins. Jpn.*, **32** [5] (1992) 616–624.
5. G. Broihanne, J. Bannister, "Cold crucible melting gets a new spin", *Mater. World*, **8** [8] (2000) 21–23.
6. G. Economos, W.D. Kingery, "Metal-ceramic interactions: II, Metal-oxide interfacial reactions at elevated temperatures", *J. Am. Ceram. Soc.*, **36** [12] (1953) 403–409.
7. A.I. Kahveci, G.E. Welsch, "Effect of oxygen on the hardness and alpha/beta phase ratio of Ti-6A1-4V alloy", *Scripta Metall.*, **20** [9] (1986)1287–1290.
8. R. Ruh, "Reactions of zirconia and titanium at elevated temperatures", *J. Am. Ceram. Soc.*, **46** [7] (1963) 301–307.
9. R.L. Saha, K.T. Jacob, "Casting of titanium and its alloys", *Defence Sci. J.*, **36** [2] (1986) 121–141.
10. R.L. Saha, T.K. Nandy, R.D.K. Misra, K.T. Jacob, "On the evaluation of stability of rare earth oxides as face coats for investment casting of titanium", *Metall. Trans. B*, **21** [3] (1990) 559–566.
11. K.I. Suzuki, S. Watakabe, K. Nishikawa, "Stability of refractory oxides for mold material of Ti-6Al-4V alloy precision casting", *J. Jpn Inst. Metal. Mater.*, **60** [8] (1996) 734–743.
12. B.C. Weber, H.J. Garrett, F.A. Mauer, M.A. Schwartz, "Observations on the stabilization of zirconia", *J. Am. Ceram. Soc.*, **39** [6] (1956) 197–206.
13. B.C. Weber, W.M. Thompson, H.O. Bielstein, M.A. Schwartz, "Ceramic crucible for melting titanium", *J. Am. Ceram. Soc.*, **40** [11] (1957) 363–373.
14. K.-F. Lin, C.-C. Lin, "Interfacial reactions between zirconia and titanium", *Scripta Mater.*, **39** [10] (1998) 1333–1338.
15. K.-F. Lin, C.-C. Lin, "Transmission electron microscope investigation of the interface between titanium and zirconia", *J. Am. Ceram. Soc.*, **82** [11] (1999) 3179–3185.
16. K.-F. Lin, C.-C. Lin, "Interfacial reactions between Ti-6Al-4V alloy and zirconia mold during casting", *J. Mater. Sci.*, **34** [23] (1999) 5899–5906.
17. K.-L. Lin, C.-C. Lin, "Ti_2ZrO phases formed in the titanium and zirconia interface after reaction at 1550 °C", *J. Am. Ceram. Soc.*, **88** [5] (2005) 1268–1272.
18. K.-L. Lin, C.-C. Lin, "Zirconia-related phases in the zirconia/titanium diffusion couple after annealing at 1100 °–1550 °C", *J. Am. Ceram. Soc.*, **88** [10] (2005) 2928–2934.
19. K.-L. Lin, C.-C. Lin, "Microstructural evolution and formation mechanism of the interface between titanium and zirconia annealed at 1550 °C", *J. Am. Ceram. Soc.*, **89** [4] (2006) 1400–1408.
20. K.-L. Lin, C.-C. Lin, "Effects of annealing temperature on microstructural development at the interface between zirconia and titanium", *J. Am. Ceram. Soc.*, **90** [3] (2007) 893–899.
21. C.-C. Lin, Y.-W. Chang, K.-L. Lin, K.-F. Lin, "Effect of yttria on interfacial reactions between titanium melt and hot-pressed yttria/zirconia composites at 1700 °C", *J. Am. Ceram. Soc.*, **91** [7] (2008) 2321–2327.
22. S.K. Kim, T.K. Kim, M.G. Kim, T.W. Hong, Kim, "Investment casting of titanium alloys with CaO crucible and $CaZrO_3$ mold", pp. 251–260 in *Lightweight Alloys for Aerospace Application*, John Wiley & Sons, Inc., 2001.
23. K.I.M. Myoung-Gyun, K.I.M. Young-Jig, "Effect of mold material and binder on metal-mold interfacial reaction for investment castings of titanium alloys", *Mater. Trans.*, **43** [4] (2002) 745–750.
24. Y.-W. Chang, C.-C. Lin, "Compositional dependence of phase formation mechanisms at the interface between titanium and calcia-stabilized zirconia at 1550 °C", *J. Am. Ceram. Soc.*, **93** [11] (2010) 3893–3901.
25. C.-H. Li, Y.-H. Gao, X.-G. Lu, W. Ding, Z.-M. Ren, K. Deng, "Interaction between the ceramic $CaZrO_3$ and the melt of titanium alloys", *Adv. Sci. Technol.*, **70** (2010) 136–140.
26. S. Schafföner, C. G. Aneziris, H. Berek, J. Hubálková, B. Rotmann, B. Friedrich, "Corrosion behavior of calcium zirconate refractories in contact with titanium aluminide melts", *J. Eur. Ceram. Soc.*, **35** [3] (2015) 1097–1106.
27. C. Wang, X. Xu, H. Yu, Y. Wen, K. Zhao, "A study of the solid electrolyte Y_2O_3-doped $CaZrO_3$", *Solid State Ionics*, **28** (1988) 542–545.
28. G. Cliff, G.W. Lorimer, "The quantitative analysis of thin specimens", *J. Microsc.*, **103** [2] (1975) 203–207.
29. T. Muromura, Y. Hinatsu, "Phase relation of ternary sys-

tem ZrO_2-CaO-Al_2O_3", *Mater. Res. Bull.*, **21** [1] (1986) 61–67
30. K. Wang, C.H. Li, Y.H. Gao, X.G. Lu, W.Z. Ding, "Thermodynamic reassessment of ZrO_2-CaO system", *J. Am. Ceram. Soc.*, **92** [5] (2009) 1098–1104.
31. J.M. Rivas Mercury, A.H. De Aza, P. Pena, "Synthesis of $CaAl_2O_4$ from powders: Particle size effect", *J. Eur. Ceram. Soc.*, **25** [14] (2005) 3269–3279.
32. S. Iftekhar, J. Grins, G. Svensson, J. Lööf, T. Jarmar, G.A. Botton, C.M. Andrei, H. Engqvist, "Phase formation of $CaAl_2O_4$ from $CaCO_3$-Al_2O_3 powder mixtures", *J. Eur. Ceram. Soc.*, **28** [4] (2008) 747–756.